REPORT DOCUMENTATION PAGE

Form Approved OMB No. 0704-0188

Public reporting burden for this collection of information is estimated to average 1 hour per response, including the time for reviewing instructions, searching existing data sources, gathering and maintaining the data needed, and completing and reviewing the collection of information. Send comments regarding this burden estimate or any other aspect of this collection of information, including suggestions for reducing this burden, to Washington Headquarters Services, Directorate for Information Operations and Reports, 1215 Jefferson Davis Highway, Suite 1204, Arlington, VA 22202-4302, and to the Office of Management and Budget, Paperwork Reduction Project (0704-0188), Washington, DC 20503.

1. AGENCY USE ONLY *(Leave blank)*	2. REPORT DATE	3. REPORT TYPE AND DATES COVERED
	22-03-2005	REPRINT

4. TITLE AND SUBTITLE

Evaluation of quasi-linear diffusion coefficients for whistler mode waves in a plasma with arbitrary density ratio.

5. FUNDING NUMBERS

PE 62601F
PR 1010
TA RS
WU A1

6. AUTHOR(S)

J.M. Albert

7. PERFORMING ORGANIZATION NAME(S) AND ADDRESS(ES)

Air Force Research Laboratory/VSBX
29 Randolph Road
Hanscom AFB, MA 01731-3010

8. PERFORMING ORGANIZATION REPORT NUMBER

AFRL-VS-HA-TR-2005-1080

9. SPONSORING/MONITORING AGENCY NAME(S) AND ADDRESS(ES)

10. SPONSORING/MONITORING AGENCY REPORT NUMBER

11. SUPPLEMENTARY NOTES

REPRINTED FROM: Journal of Geophysical Research, Vol. 110, A03218, doi:10.1029/2004JA010844, 2005

12a. DISTRIBUTION AVAILABILITY STATEMENT

Approved for public release; distribution unlimited.

12b. DISTRIBUTION CODE

13. ABSTRACT *(Maximum 200 words)*

Techniques are presented for efficiently evaluating quasi-linear diffusion coefficients for whistler mode waves propagating according to the full cold plasma index of refraction. In particular, the density ratio ω_{pe}/Ω_e can be small, which favors energy diffusion. This generalizes an approach, previously used for high-density hiss and electromagnetic ion cyclotron waves, of identifying (and omitting) ranges of wavenormal angle θ that are incompatible with cyclotron resonant frequencies ω occurring between sharp cutoffs of the modeled wave frequency spectrum. This requires a detailed analysis of the maximum and manimum values of the refractive index as a function of ω and θ, as has previously been performed in the high-density approximation. Sample calculations show the effect of low-density ratio on the pitch angle and energy diffusion coefficients modeling the effect of chorus waves on radiation belt electrons. The high-density approximation turns out to be quite robust, especially when the upper frequency cutoff is small compared with Ω_e. The techniques greatly reduce the amount of computation needed for a sample calculation, while taking into account all resonant harmonic numbers n up to $\pm \infty$.

14. SUBJECT TERMS

Whistler waves
Quasilinear diffusion
Radiation belt electrons

15. NUMBER OF PAGES

16. PRICE CODE

17. SECURITY CLASSIFICATION OF REPORT	18. SECURITY CLASSIFICATION OF THIS PAGE	19. SECURITY CLASSIFICATION OF ABSTRACT	20. LIMITATION OF ABSTRACT
UNCL	UNCL	UNCL	UNL

AFRL-VS-HA-TR-2005-1080

JOURNAL OF GEOPHYSICAL RESEARCH, VOL. 110, A03218, doi:10.1029/2004JA010844, 2005

Evaluation of quasi-linear diffusion coefficients for whistler mode waves in a plasma with arbitrary density ratio

J. M. Albert

Air Force Research Laboratory, Space Vehicles Directorate, Hanscom Air Force Base, Massachusetts, USA

Received 15 October 2004; revised 9 December 2004; accepted 22 December 2004; published 22 March 2005.

[1] Techniques are presented for efficiently evaluating quasi-linear diffusion coefficients for whistler mode waves propagating according to the full cold plasma index of refraction. In particular, the density ratio ω_{pe}/Ω_e can be small, which favors energy diffusion. This generalizes an approach, previously used for high-density hiss and electromagnetic ion cyclotron waves, of identifying (and omitting) ranges of wavenormal angle θ that are incompatible with cyclotron resonant frequencies ω occurring between sharp cutoffs of the modeled wave frequency spectrum. This requires a detailed analysis of the maximum and minimum values of the refractive index as a function of ω and θ, as has previously been performed in the high-density approximation. Sample calculations show the effect of low-density ratio on the pitch angle and energy diffusion coefficients modeling the effect of chorus waves on radiation belt electrons. The high-density approximation turns out to be quite robust, especially when the upper frequency cutoff is small compared with Ω_e. The techniques greatly reduce the amount of computation needed for a sample calculation, while taking into account all resonant harmonic numbers n up to $\pm\infty$.

Citation: Albert, J. M. (2005), Evaluation of quasi-linear diffusion coefficients for whistler mode waves in a plasma with arbitrary density ratio, *J. Geophys. Res.*, *110*, A03218, doi:10.1029/2004JA010844.

1. Introduction

[2] Cyclotron-resonant wave-particle interactions are currently a leading candidate for understanding the behavior of outer radiation belt electrons following magnetic storms. In particular, *Summers et al.* [1998] proposed that energization by dawnside whistler mode chorus waves, combined with pitch angle scattering by duskside electromagnetic ion cyclotron (EMIC) waves, might account for the observed distributions of energetic electrons. By analyzing the path in velocity space followed by an electron as it maintains primary ($n = -1$) resonance with a field-aligned wave, it was found that energy diffusion is favored by the low ($\sim$1) values of the density ratio, ω_{pe}/Ω_e, found outside the plasmasphere. *Horne et al.* [2003] presented detailed quasi-linear diffusion coefficients for low-density chorus and confirmed the effectiveness of energy diffusion, although these calculations were restricted to local (equatorial) interactions. *Horne et al.* [2005] presented bounce-averaged results, using realistic wave models. These calculations were performed using two different approaches, one of which is described by *Glauert and Horne* [2005] and one of which is described here.

[3] Whistler mode chorus waves are observed to have fine structure, including time-evolving frequencies [e.g., *Santolik et al.*, 2003] and are associated with the strongly nonlinear processes of particle phase bunching and phase trapping (see the review by *Sazhin and Hayakawa* [1992], and also *Smith and Nunn* [1998], *Albert* [2000, 2001, 2002], and *Trakhtengerts et al.* [2003]). However, it is assumed here that quasi-linear theory is a meaningful description of the long-term effect of fully formed waves on high-energy particles [*Summers et al.*, 1998; *Summers and Ma*, 2000; *Horne et al.*, 2003, 2005].

[4] Previous calculations of quasi-linear diffusion have generally relied on the high-density approximation introduced by *Lyons* [1974b], which leads to a greatly simplified form of the index of refraction μ. This allows a characterization of the resonant frequencies at each wavenormal angle. Since the diffusion coefficients are infinite sums of integrals over wavenormal angle θ (and then bounce averaged), it turns out to be possible, and extremely beneficial, to restrict the range of the integrals over θ. This analysis has been carried out for whistler mode plasmaspheric hiss [*Albert*, 1999, hereinafter referred to as Paper 1] and for EMIC waves [*Albert*, 2003, hereinafter referred to as Paper 2], using the high-density approximation. This paper generalizes that approach to whistler mode waves with arbitrary values of the density ratio.

[5] Section 2 presents the quasi-linear diffusion coefficients (pitch angle, momentum, and mixed), in a form that generalizes the formulas of *Lyons* [1974b] to relativistic test particles, general μ, and arbitrary wavenormal angle and frequency profiles. Section 3 expresses the cyclotron resonance condition in terms of $1/\mu^2$ (denoted by Ψ) and a function V which contains all the dependence on parameters of the test particle and briefly discusses the simple geometric behavior of V as a function of ω. Section 4 presents a detailed algebraic, geometrical, and numerical analysis of the full two-component cold plasma whistler-mode refractive index as a function of ω. Particular attention is paid to

This paper is not subject to U.S. copyright.
Published in 2005 by the American Geophysical Union.

20050919 007

DISTRIBUTION STATEMENT A
Approved for Public Release
Distribution Unlimited

the maximum and minimum values over a fixed ω range and how these values vary with θ. Several bounds and approximations are discussed, including the high-density approximation and a novel factorization. Section 5 identifies values of θ for which the maximum-to-minimum ranges of $V(\omega)$ and $\Psi(\omega)$ do not overlap; for such θ values, there can be no resonances. For large-enough harmonic number $|n|$ there will be no resonances for any θ (since V_{max} becomes less than Ψ_{min}), which cuts off the sum over $n = -\infty$ to ∞. Additional tests based on the curvatures of $V(\omega)$ and $\Psi(\omega)$ are also developed. Finally, the dependence on latitude λ is considered, which leads to tests for λ ranges that have no resonances for any θ or n. In section 6 the preceding analysis is used for $n \leq 0$ to isolate, or bracket, the resonant frequencies which do exist so that they can be found quickly and easily by a generic one-dimensional (1-D) root-finding algorithm. This bracketing cannot always be done for $n > 0$, as explained, and alternative procedures are discussed. Section 7 discusses the ratio $D_{pp}/D_{\alpha\alpha}$ and explores why this ratio should increase as ω_{pe}/Ω_e decreases. Section 8 explores the reliability of the high-density approximation for different values of ω_{pe}/Ω_e and quantifies the gain in computational efficiency made possible by the methods of this paper. A summary is given in section 9.

2. Quasi-Linear Diffusion Coefficients

[6] The resonance condition for a diffusing particle is

$$\omega - k_\parallel v_\parallel = \omega_n, \quad \omega_n \equiv sn\Omega_c/\gamma, \tag{1}$$

where n is an integer, $s = \pm 1$ is the sign of the charge of the particle, $\Omega_c = |q|B_o/mc$ is its local nonrelativistic gyrofrequency, and γ is its relativistic factor. The local pitch angle of the particle is α, the index of refraction is $\mu \equiv kc/\omega$, the wavenormal angle is θ, and x will denote $\tan\theta$ throughout.

[7] The underlying physics of the diffusion coefficients used here is identical to that of *Lyons* [1974b], except for the extension to relativistic test particles (as briefly discussed by *Lyons* [1974a]). However, the frequency and wavenormal angle profiles $B^2(\omega)$ and $g_\omega(\theta)$ are kept general, and we also postpone specifying the form of the refractive index. The normalized diffusion kernel for $D_{\alpha\alpha}$ can be written as

$$\mathcal{D}^{nx}_{\alpha\alpha} = \frac{\pi}{2}\frac{\Omega_c}{\Delta\omega}\frac{\cos^2\theta}{\left|v_\parallel/c\right|^3}\Phi_n^2\frac{\left(-\sin^2\alpha + \omega_n/\omega\right)^2}{\left|1 - \left(\partial\omega/\partial k_\parallel\right)_x/v_\parallel\right|}G_1G_2, \tag{2}$$

where $G_1(\omega) = (\Delta\omega)B^2(\omega)/\int B^2(\omega')d\omega'$, and

$$G_2(\omega,\theta) = \frac{g_\omega(\theta)}{\int g_\omega(\theta')\mu^2\left|\mu + \omega\partial\mu/\partial\omega\right|\sin\theta' d\theta'}. \tag{3}$$

The normalization $\Delta\omega$ is arbitrary, but it is convenient to use a value characteristic of the width of $B^2(\omega)$. Then $\mathcal{D}^{nx}_{\alpha p}$, $\mathcal{D}^{nx}_{p\alpha}$, and $\mathcal{D}^{nx}_{pp}$ are given by

$$\frac{\mathcal{D}^{nx}_{\alpha p}}{\mathcal{D}^{nx}_{\alpha\alpha}} = \frac{\sin\alpha\cos\alpha}{-\sin^2\alpha + \omega_n/\omega}, \quad \frac{\mathcal{D}^{nx}_{pp}}{\mathcal{D}^{nx}_{\alpha\alpha}} = \left(\frac{\mathcal{D}^{nx}_{\alpha p}}{\mathcal{D}^{nx}_{\alpha\alpha}}\right)^2. \tag{4}$$

The normalized diffusion coefficients themselves are then

$$\mathcal{D}_{\alpha\alpha} = \sum_n \int x\mathcal{D}^{nx}_{\alpha\alpha}dx = \sum_n \int x\mathcal{D}^{nx}_{\alpha\alpha}\left|\frac{\partial x}{\partial\omega}\right|_{res} d\omega, \tag{5}$$

where n ranges over $\pm\infty$, and similarly for $\mathcal{D}_{\alpha p}$ and $\mathcal{D}_{pp}$. The term Φ_n^2 above is exactly as given in equation (9) of *Lyons* [1974b], except that the arguments of the Bessel functions therein become $[nx\tan\alpha(\omega - \omega_n)/\omega_n]$ (as in Paper 1) to account for relativistic factors. The partial derivatives above may be expressed in terms of derivatives of $\mu(\omega, \theta)$ by

$$\frac{1}{v_\parallel}\left(\frac{\partial\omega}{\partial k_\parallel}\right)_x = \frac{\omega}{\omega - \omega_n}\frac{\mu}{\mu + \omega\partial\mu/\partial\omega} \tag{6}$$

and

$$\left.\frac{\partial x}{\partial\omega}\right|_{res} = -\frac{\mu\omega_n/[\omega(\omega - \omega_n)] - \partial\mu/\partial\omega}{\mu\sin\theta\cos\theta - \partial\mu/\partial x}. \tag{7}$$

The physical momentum diffusion coefficients D are equal to the normalized quantities $\mathcal{D}$ multiplied by $\Omega_c(B^2_{wave}/B^2_o)(mv)^2$. Finally, the bounce-averaged diffusion coefficients are $\langle D_{\alpha_0\alpha_0}\rangle = \int D_{\alpha\alpha}(\partial\alpha_0/\partial\alpha)^2\, dt/\tau_b$, $\langle D_{\alpha_0 p}\rangle = \int D_{\alpha p}(\partial\alpha_0/\partial\alpha)\, dt/\tau_b$, and $\langle D_{pp}\rangle = \int D_{pp}dt/\tau_b$, where τ_b is the bounce time. These may be converted to integrals over latitude (as detailed for $D_{\alpha\alpha}$ by *Lyons et al.* [1972] for a dipole field) or over α (which may give better numerical behavior near the mirror point).

[8] It has become standard to model the power spectrum $B^2(\omega)$ as proportional to a gaussian truncated at ω_{LC} and ω_{UC} and the wavenormal angle profile $g_\omega(x)$ as a gaussian truncated at x_{min} and x_{max}. Then, taking $\Delta\omega$ equal to the frequency width $\delta\omega$,

$$G_1 = \frac{2}{\sqrt{\pi}}\frac{\exp\left[-(\omega - \omega_m)^2/\delta\omega^2\right]}{\mathrm{erf}[(\omega_{UC} - \omega_m)/\delta\omega] + \mathrm{erf}[(\omega_m - \omega_{LC})/\delta\omega]}, \tag{8}$$

and, with the high-density approximation for μ (discussed below),

$$G_2 = \left(\frac{M}{1 + M}\frac{\Omega_e^2}{\omega_{pe}^2}\right)^{3/2}\frac{\exp\left[-(x - x_m)^2/x_w^2\right]}{I(\omega)}, \tag{9}$$

where $M = m_e/m_i$ and $I(\omega)$ (with $x_{min} = 0$) is defined by *Lyons* [1974b]. Nonrelativistically, these expressions all reduce exactly to the formulas given there. The choice of gaussians is not crucial, but the existence of lower and upper frequency cutoffs, ω_{LC} and ω_{UC}, is essential for the analysis. As in Papers 1 and 2, the frequency cutoffs can be used to derive restrictions on θ, which limit the range of the x integration in equation (5). Thus by preidentifying ranges of θ for which ω is outside the cutoffs, the amount of computation needed to obtain D may be drastically reduced.

3. Resonance Condition

[9] Despite the formidable appearance of the expressions for the diffusion coefficients, the only quantity not straightforward to evaluate is the resonant frequency $\omega(\theta)$, which is needed if $\mathcal{D}^{nx}$ is integrated over θ rather than ω.

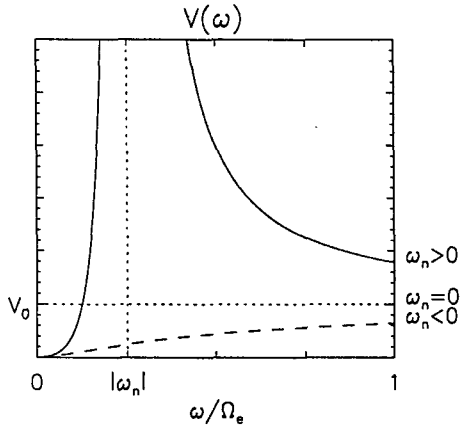

Figure 1. The function $V(\omega)$ at fixed θ, with $n = 0$ (dotted curve), $n = 1$ (dashed curve), and $n = -1$ (solid curve), for an electron with $\gamma = 4$ and $(v_\parallel^2/c^2)\cos^2\theta = 0.5$.

[10] The resonance condition, equation (1), may be written as $V(\omega, \theta) = \Psi(\omega, \theta)$ where, similar to Papers 1 and 2,

$$V \equiv \frac{v^2}{c^2}\frac{\omega^2}{(\omega - \omega_n)^2}\cos^2\alpha\cos^2\theta, \quad \Psi \equiv \frac{1}{\mu^2}. \tag{10}$$

There is a loss of sign information in going from equation (1) to $V = \Psi$ (via squaring), but it is assumed that for every wave mode with positive $k_\parallel/k$ there is a mode of equal amplitude with negative $k_\parallel/k$, so any solution of $V = \Psi$ corresponds to a solution of (1). Furthermore, the particle distribution is assumed to be the same for $v_\parallel$ positive and $v_\parallel$ negative. This definition of Ψ differs slightly from that of *Lyons* [1974b] and Papers 1 and 2, where it denoted the high-density limit of $[(\omega_{pe}^2/\Omega_e^2)(1 + M)/M]/\mu^2$. This limit will be discussed in the next section.

[11] The geometric properties of $V(\omega)$ at fixed θ were established in Paper 1 and are shown in Figure 1. For $n = 0$, $V(\omega)$ has the constant value $V_0 \equiv (v_\parallel^2/c^2)\cos^2\theta$. For ω_n positive, V always has positive curvature and is increasing for $\omega < \omega_n$ and decreasing and bounded below by V_0 for $\omega > \omega_n$. For ω_n negative, $V(\omega)$ is strictly increasing but bounded above by V_0 and has positive curvature $\partial^2 V/\partial\omega^2$ for $\omega < |\omega_n|/2$ and negative curvature for $\omega > |\omega_n|/2$. The properties of Ψ are discussed in the next section.

4. Index of Refraction

[12] The standard wave coefficients [*Stix*, 1962] for a cold pure electron-proton plasma are

$$\left\{\begin{matrix} R \\ L \end{matrix}\right\} = 1 \pm \frac{\omega_{pe}^2}{\Omega_e\omega}\frac{1 + M}{1 - M \mp (\omega/\Omega_e - \Omega_i/\omega)},$$
$$P = 1 - \frac{\omega_{pe}^2}{\omega^2}(1 + M), \; S = \frac{R + L}{2}, \; D = \frac{R - L}{2}, \tag{11}$$

and the full expression for Ψ can be written as

$$\Psi = \left\{(RL - PS)\sin^2\theta + 2PS \pm \sqrt{(RL - PS)^2\sin^4\theta + 4P^2D^2\cos^2\theta}\right\}/2PRL. \tag{12}$$

The choice $\pm$ in equation (12) determines the labeling of the wave as "R mode" (+) or "L mode" (−), but the wavenormal surfaces exchange labels (or, as *Stix* [1962] puts it, the labels exchange wavenormal surfaces) when crossing $P = 0$ or $D = 0$. Here only waves with $\omega < \Omega_e$ and $\omega < \omega_{pe}$ are considered, although ω_{pe} is allowed to be less than Ω_e. Thus P is always negative, but D becomes negative for $\omega < \Omega_i$ (to lowest order in M). Therefore $\pm$ is chosen to be "+" when $D > 0$, for R-mode polarization, and "−" when $D < 0$, for continuity.

[13] Usually, μ^2 is treated as a function of θ at fixed ω; here, Figure 2 shows Ψ versus ω at fixed θ (and fixed ω_{pe}/Ω_e). For each curve, it can be shown algebraically that $\partial\Psi/\partial\omega = 0$ at $\omega = 0$ so that the behavior of Ψ near zero is determined by its curvature $\partial^2\Psi/\partial\omega^2$ there. For small and moderate θ this curvature is positive, so $\Psi(\omega)$ starts out increasing but soon develops negative curvature, eventually peaks (before reaching $\Omega_e/2$), and then decreases to zero while retaining negative curvature. These curves each have one internal maximum and no internal minima. For large θ, Ψ starts out with with negative curvature and declines monotonically to zero, with no internal maxima. The two classes of curves are separated by the curve that has zero curvature at $\omega = 0$; this occurs for

$$\sin^2\theta_{sep} = \left.\frac{2(R')^2}{RR''}\right|_{\omega=0} \approx \frac{\omega_{pe}^2/\Omega_e^2}{M + \omega_{pe}^2/\Omega_e^2}, \tag{13}$$

which gives θ very close to 90° unless $\omega_{pe}/\Omega_e \sim \sqrt{M}$ or less. This is shown as the thick curve in Figures 2c and 2d and is observed to cross zero at frequency ω_{sep} near $\Omega_{gm} \equiv (\Omega_e\Omega_i)^{1/2}$ (the geometric mean of Ω_e and Ω_i).

[14] In general, Ψ reaches zero at the frequency given by the expression $\tan^2\theta = -P/S$ [*Stix*, 1962]. Using this to find the Ψ curve that reaches zero right at Ω_{gm}, for which $S = 1$, yields

$$\sin^2\theta_{gm} = \left.\frac{-P}{1 - P}\right|_{\Omega_{gm}} \approx \frac{\omega_{pe}^2/\Omega_e^2 - M}{\omega_{pe}^2/\Omega_e^2}, \tag{14}$$

which is slightly less than $\sin^2\theta_{sep}$. This is shown by the upper dashed curve in Figure 2d. The Ψ curve for $\sin^2\theta = 1$ crosses zero at the lower hybrid resonance, ω_{LH}, where $S = 0$. Thus for $\omega > \omega_{LH}$ there is some maximum θ, the well-known resonance cone angle, beyond which Ψ becomes negative. This Ψ curve is the lower dashed curve in Figure 2d. Since $\sin^2\theta_{gm} < \sin^2\theta_{sep} < 1$, the separating curve crosses zero at ω_{sep} with $\omega_{LH} < \omega_{sep} < \Omega_{gm}$. (A good approximation to ω_{LH} is

$$\Omega_{gm}\sqrt{\frac{M + \omega_{pe}^2/\Omega_e^2}{1 + \omega_{pe}^2/\Omega_e^2}},$$

which is always less than Ω_{gm}.) Ω_{gm} will also play an important role below.

[15] As θ increases, the Ψ curves generally shift left and down, and ω_{peak} and $\Psi(\omega_{peak})$ are decreasing functions of θ as confirmed by the falling curves in Figures 3a and 3b. From a different point of view, if for some value of θ the slope $\partial\Psi/\partial\omega$ at fixed ω is positive, the slope decreases to

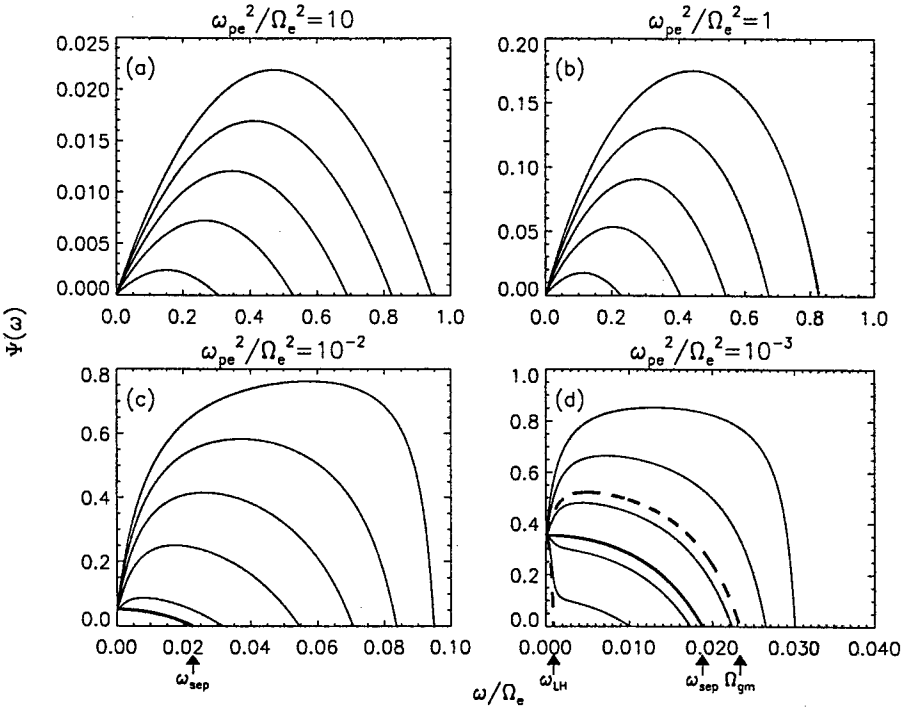

Figure 2. The function $\Psi(\omega)$ at fixed values of ω_{pe}^2/Ω_e^2, for $\sin^2\theta = 0.1$ (top curves), 0.3, 0.5, 0.7, and 0.9 (bottom curves). The thick solid curves in Figures 2c and 2d are for θ_{sep} and have zero curvature at $\omega = 0$. Also shown in Figure 2d are the curves for θ_{gm}, which crosses zero at Ω_{gm} (upper dashed curve), and for $\theta = \pi/2$, which crosses zero at ω_{LH} (lower dashed curve).

negative values as θ increases. Extensive numerical tests show that once this slope becomes negative it stays negative so that there is (at most) one value of θ for which Ψ peaks at any fixed ω.

[16] The rising curves in Figure 3a show the inflection point frequency, where Ψ switches from positive curvature to negative curvature. (The values ω_{peak} and ω_{infl} are undefined when the curvature at $\omega = 0$ becomes zero, at $\sin^2\theta_{sep}$.) This ω_{infl} is usually an increasing function of θ, although it must stay less than ω_{peak}. In fact, Figure 3c indicates that ω_{infl} is always less than ω_{LH}.

4.1. High-Density Approximation

[17] In this and the next subsection, two alternate forms of Ψ are presented which will be useful: the high-density approximation and a novel factorization of Ψ. In the high-density limit, $\omega_{pe}^2/\Omega_e^2 \gg \omega/\Omega_e$, simply dropping the leading "1's" in the definitions of R, L, and P leads to the much simpler expression

$$\Psi^{HD} = \frac{\Omega_e^2}{\omega_{pe}^2}\frac{M}{1+M}\left\{1 - \frac{\omega^2}{\Omega_e\Omega_i} - \frac{\sin^2\theta}{2} + \sqrt{\frac{\sin^4\theta}{4} + \frac{\omega^2}{\Omega_i^2}(1-M)^2\cos^2\theta}\right\} \quad (15)$$

Apart from the terms in front of the braces, Ψ^{HD} is the form introduced by *Lyons* [1974b] and used for quasi-linear diffusion coefficient calculations almost exclusively ever since.

[18] It is proved in Appendix A that $\Psi < \Psi^{HD}$. Since Ψ^{HD} admits explicit analytical expressions for ω_{peak} and $\Psi(\omega_{peak})$, it provides a useful upper bound on the true Ψ_{max}.

4.2. A Factorization of Ψ

[19] A different form of the expression for Ψ is suggested by defining $\hat{\omega} = \omega/\Omega_e$, and $\hat{R} = R\hat{\omega}$ and similarly for $\hat{L}$, $\hat{P}$, $\hat{S}$, and $\hat{D}$. Then the full Ψ, with the same choices of $\pm$ as for equation (12), can be written as

$$\Psi = \left(\frac{\hat{D}\hat{\omega}}{\hat{R}}\right)\left\{\frac{1}{\hat{L}}\left[\frac{\hat{R}\hat{L}-\hat{P}\hat{S}}{\hat{D}}\frac{\sin^2\theta}{2\hat{P}} + \frac{\hat{S}}{\hat{D}} - \sqrt{\left(\frac{\hat{R}\hat{L}-\hat{P}\hat{S}}{\hat{D}}\right)^2\frac{\sin^4\theta}{4\hat{P}^2} + \cos^2\theta}\right]\right\}. \quad (16)$$

The benefit of writing Ψ in this form is that for $\omega > \Omega_{gm}$, the first term in parentheses, denoted by Ψ_+, is a strictly increasing function of $\hat{\omega}$, while the term in braces, denoted by Ψ_-, is a strictly decreasing function of $\hat{\omega}$. A proof is outlined by *Albert* [2004]. The monotonicity of Ψ_+ and Ψ_- immediately gives the bounds

$$\Psi_+(\omega_{LC})\Psi_-(\omega_{UC}) < \Psi(\omega) < \Psi_+(\omega_{UC})\Psi_-(\omega_{LC}), \quad (17)$$

which will be close estimates if ω_{LC} is close to ω_{UC}. The lower bound is superfluous because the minimum value of Ψ is known to occur at either ω_{LC} or ω_{UC}, but the upper bound is valuable when ω_{peak} lies between ω_{LC} and ω_{UC}, as discussed in section 5.

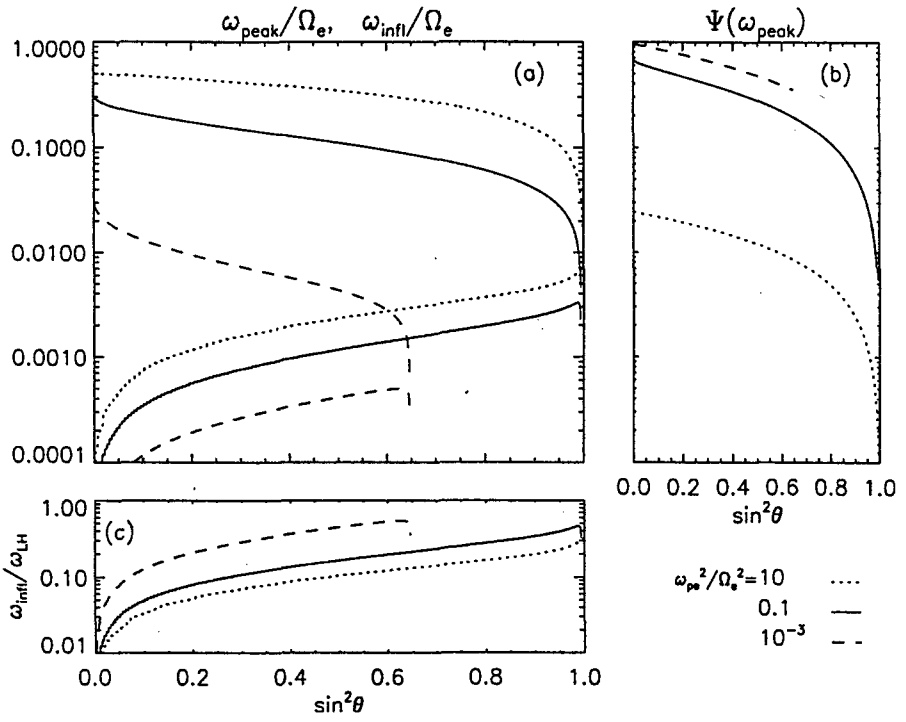

Figure 3. (a) The frequencies, normalized by Ω_e, where Ψ has a peak (falling curves) or inflection point (rising curves), for $\omega_{pe}^2/\Omega_e^2 = 10$ (dotted curves), 0.1 (solid curves), 10^{-3} (dashed curves), versus $\sin^2\theta$. (b) The values of Ψ at its peak. (c) The inflection frequencies normalized by ω_{LH}.

[20] It is worth noting that the heavy ion approximation $M = 0$ reduces $(\hat{R}\hat{L} - \hat{P}\hat{S})/\hat{D}$ to 1, which simplifies equation (16) considerably. It is proved in Appendix A that $\Psi^{(M=0)} < \Psi$ so that

$$\Psi^{(M=0)} < \Psi < \Psi^{HD}. \tag{18}$$

Also, $\Psi_+^{(M=0)}$ and $\Psi_-^{(M=0)}$ are monotonic increasing and decreasing, respectively, for all frequencies $0 < \omega < \min[\Omega_e, \omega_{pe}]$.

[21] Figure 4 shows the dependence of the three versions of Ψ on ω for 12 different combinations of ω_{pe}/Ω_e and θ. In each double plot, the entire range $0 \le \omega \le \Omega_e$ is shown, as well as an expanded view of the range $0 \le \omega \le \Omega_{gm}$. The heavy dashed line is the full, exact Ψ. Also shown in each plot is Ψ^{HD} as a solid line that always lies above the full Ψ and $\Psi^{(M=0)}$ as a solid line that always lies below the full Ψ but is in several cases almost indistinguishable from it. The vertical scale is indicated by listing the peak value of Ψ^{HD}; this can be greater than 1, but the full expression for Ψ is always less than 1.

5. Eliminating Ranges of θ

[22] If the integrals in equation (5) are performed over ω, the resonance condition gives an easily solved quadratic equation for $\cos^2\theta$ as a function of ω. Integrating over $x = \tan\theta$ instead involves the more difficult problem of solving for $\omega(\theta)$ but offers greatly improved efficiency by cutting down the required range of integration or, in favorable cases, eliminating θ integrals altogether. As in Papers 1 and 2, the strategy is to circumvent the complicated algebraic dependence of Ψ on ω by considering Ψ geometrically, using the properties discussed in the previous section, while exploiting the relatively simple algebraic dependence of Ψ on θ.

5.1. Overlap of Maximum and Minimum Values

[23] The fundamental geometric idea is that at fixed θ, $V(\omega)$ and $\Psi(\omega)$ cannot intersect if V is larger than Ψ or if V is smaller than Ψ for all ω between ω_{LC} and ω_{UC}. (The latter case is illustrated in Figure 5a.) Such θ values yield no resonances and can be skipped in the integration for the diffusion coefficients. The prescription is thus

$$\text{skip } \theta: \; V_{max} < \Psi_{min} \text{ or } V_{min} > \Psi_{max}. \tag{19}$$

Once the values of ω that maximize and minimize V and Ψ between ω_{LC} and ω_{UC} are determined for fixed θ, writing out the conditions in (19) directly gives quadratic inequalities of the form $A\cos^4\theta + B\cos^2\theta + C > 0$. As in Paper 1 (Appendix A1) or Paper 2 (Appendix B), these inequalities are readily solved for ranges of θ which may be skipped.

5.1.1. V_{min} and V_{max}

[24] The geometric behavior of V, shown in Figure 1, makes it easy to determine V_{min} and V_{max} (just as in Papers 1 and 2). For $\omega_n = 0$, they are both just V_0. For $\omega_n < 0$, V_{min} is $V(\omega_{LC})$ and V_{max} is $V(\omega_{UC})$. For $0 < \omega_n < \omega_{LC}$, V_{min} is $V(\omega_{UC})$ and V_{max} is $V(\omega_{LC})$, while for $\omega_{UC} < \omega_n$, V_{min} is $V(\omega_{LC})$ and V_{max} is $V(\omega_{UC})$. If $\omega_{LC} < \omega_n < \omega_{UC}$, V_{min} is the smaller of $V(\omega_{LC})$ and $V(\omega_{UC})$ and V_{max} is infinite.

5.1.2. The Condition $V_{max} < \Psi_{min}$

[25] Since Ψ_{min} is the smaller of $\Psi(\omega_{LC})$ and $\Psi(\omega_{UC})$, the condition $V_{max} < \Psi_{min}$ is satisfied by θ ranges where both

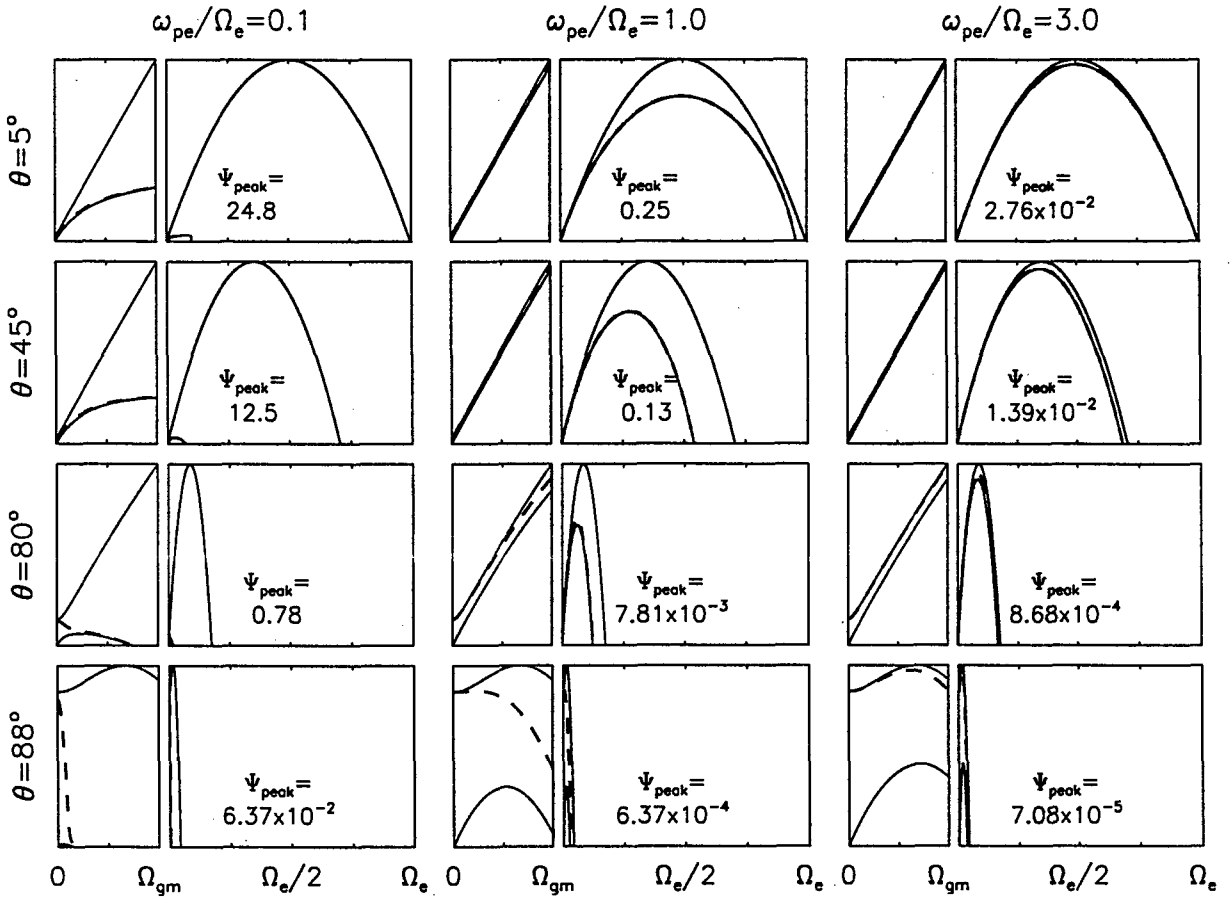

Figure 4. The function $\Psi(\omega)$ (dashed curves), for different values of θ and ω_{pe}/Ω_e. Also shown are the high density approximation (upper solid curves) and the $M = 0$ approximation (lower solid curves). For better resolution, the ranges 0 to Ω_{gm} and 0 to Ω_e are shown separately. The vertical scale goes from 0 to the peak value of Ψ^{HD}, which is indicated in each figure. For ω_{pe}/Ω_e as low as 1, the high-density approximation is quite good for small ω/Ω_e unless θ is very large.

$V_{max} < \Psi(\omega_{LC})$ and $V_{max} < \Psi(\omega_{UC})$. Note that for $\omega_n < 0$ or $\omega_n > \omega_{UC}$, V_{max} is $V(\omega_{UC})$ and decreases with increasing $|n|$. Therefore for $|n|$ large enough, V_{max} will always be less than Ψ_{min}, which gives a systematic means of limiting the doubly infinite number of n values in the sum of equation (5).

5.1.3. The Condition $V_{min} > \Psi_{max}$

[26] This condition is more complicated, because Ψ_{max} depends on θ. From Figure 3a, ω_{peak} decreases as θ increases and there is a unique value $\theta = \Theta_{UC}$ (found numerically) for which Ψ peaks at ω_{UC}, so $\Psi_{max} = \Psi(\omega_{UC})$ for $\theta \leq \Theta_{UC}$. Similarly, there is a larger value Θ_{LC} for which Ψ peaks at ω_{LC}, so $\Psi_{max} = \Psi(\omega_{LC})$ for $\theta \geq \Theta_{LC}$. (Thus $\omega_{LC} < \omega_{UC}$ but $\Theta_{LC} > \Theta_{UC}$.) For either $\theta < \Theta_{UC}$ or $\theta > \Theta_{LC}$ the condition $V_{min} > \Psi_{max}$ specifies quadratics for $\cos^2\theta$.

[27] For θ between Θ_{UC} and Θ_{LC}, the maximum of Ψ occurs somewhere between ω_{UC} and ω_{LC}, and no simple, exact characterization has been found. However, any function $\tilde{\Psi}$ which is an upper bound of Ψ may be used, since then $V_{min} > \tilde{\Psi}_{max}$ guarantees $V_{min} > \Psi_{max}$. One immediate (over)estimate is $\Psi(\omega_{UC}, \Theta_{UC})$, since the peak value of Ψ decreases as θ increases (see Figure 3b). Note that for $\theta = \Theta_{LC}$, Ψ_{peak} is actually $\Psi_+(\omega_{LC})\,\Psi_-(\omega_{LC}, \Theta_{LC})$, while the estimate just given is $\Psi_+(\omega_{UC})\,\Psi_-(\omega_{UC}, \Theta_{UC})$ and the upper bound given in equation (17) is $\Psi_+(\omega_{UC})\Psi_-(\omega_{LC}, \Theta_{LC})$. Neither estimate dominates the other, so both should be used to narrow down the retained θ ranges. The upper bound Ψ^{HD} can be used as well.

5.2. Curvature

[28] The conditions in equation (19), based on the maximum and minimum values of of $V(\omega)$ and $\Psi(\omega)$, may be augmented by geometrically simple ideas involving their curvature. For $\omega > \omega_{LH}$, Ψ has negative curvature (concave downward) and V has positive curvature (concave upward) on either side of ω_n (for ω_n positive) or for $\omega < |\omega_n|/2$ (for ω_n negative). Now suppose $V(\omega_{LC}) < \Psi(\omega_{LC})$ and $V(\omega_{UC}) < \Psi(\omega_{UC})$ for some range of θ, as illustrated in Figure 5b. Since $V(\omega)$ and $\Psi(\omega)$ "curve away from each other," there can be no intersections between ω_{LC} and ω_{UC}. The corresponding θ ranges can be found from quadratics as above.

[29] Similar considerations apply to the combination V concave downward, Ψ concave upward, with $V(\omega_{LC}) > \Psi(\omega_{LC})$ and $V(\omega_{UC}) > \Psi(\omega_{UC})$. However, this requires both $\omega_n < 0$, $\omega > |\omega_n|/2$ (for the V curvature) and $\omega < \omega_{LH}$ (for the

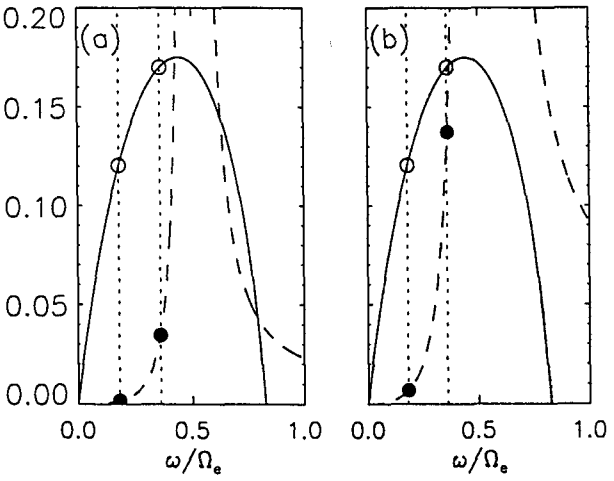

Figure 5. $V(\omega)$ and $\Psi(\omega)$ with $\omega_{pe}^2/\Omega_e^2 = 1$ and $\sin^2\theta = 0.1$, for a 0.5 MeV electron with $n = -1$. Also shown for illustration are $\omega_{LC} = 0.18$ and $\omega_{UC} = 0.36$. Maximum and minimum values are shown by filled circles for V and open circles for Ψ. (a) $\alpha = 85°$. In this case, $V_{max} < \Psi_{min}$ and there is no resonance between the cutoffs. (b) $\alpha = 80°$. Here, V_{max} is not less than Ψ_{min}, but the lack of resonance between the cutoffs may be detected by the curvature argument of section 5.2.

Ψ curvature) so that $\gamma > |n|/2\sqrt{M}$ or $E > 10$ MeV for electrons.

5.3. Ranges of λ

[30] The diffusion coefficients may be bounce averaged according to $\langle D_{\alpha_0}\alpha_0\rangle = (1/\tau_b)\int D_{\alpha\alpha}(\partial\alpha_0/\partial\alpha)^2 ds/v_\parallel$, etc., and the integration along a field line may be carried out over latitude λ [*Lyons et al.*, 1972] or local pitch angle α. The preceding approach may be extended to eliminate unnecessary ranges of λ (or α), as follows. Consider V and Ψ as functions of $\hat{\omega} = \omega/\Omega_e$ so that the curve of $V(\hat{\omega})$ at fixed θ is λ-dependent only through α and $\Psi(\hat{\omega})$ is λ-dependent only through ω_{pe}/Ω_e. V is a strictly decreasing function of λ, while the λ dependence of Ψ is more complicated but $\hat{\Psi} = (\omega_{pe}^2/\Omega_e^2)\Psi$ strictly increases with ω_{pe}/Ω_e, as shown in Figure 6 and proved in Appendix A. Then the resonance condition for a particle with equatorial pitch angle α_0 can be rewritten slightly as $\hat{V} = \hat{\Psi}$, where

$$\hat{V} \equiv \frac{v^2}{c^2}\frac{\omega_{pe0}^2}{\Omega_{e0}^2}\left[\frac{1 - h\sin^2\alpha_0}{h^2}\right]\frac{\hat{\omega}^2}{(\hat{\omega} - \hat{\omega}_n)^2}\cos^2\theta \qquad (20)$$

and $h(\lambda)$ is Ω_e divided by its equatorial value Ω_{e0}. The bracketed combination, denoted by $H(\lambda)$, strictly decreases as λ increases. Any λ dependence of ω_{pe}, ω_{LC}, and ω_{UC} will be ignored for simplicity, though this can be generalized. Then the normalized frequency cutoffs ω_{LC}/Ω_e and ω_{UC}/Ω_e are bounded below and above, respectively, by $\hat{\omega}_{LC} \equiv \omega_{LC}/\Omega_e(\lambda_{max})$ and $\hat{\omega}_{UC} \equiv \omega_{UC}/\Omega_e(\lambda_{min})$, where λ_{min} and λ_{max} are determined by both α_0 and the range of the waves.

[31] It is now straightforward to derive conditions for λ ranges which guarantee $\hat{V}_{max} < \hat{\Psi}_{min}$ or $\hat{V}_{min} > \hat{\Psi}_{max}$ so that these ranges need not be included in the bounce averaging. The maximum and minimum values must be found over ranges of θ, λ, and $\hat{\omega}$. For simplicity, consider the case $n = 0$, for which $\hat{V}$ is independent of $\hat{\omega}$. An underestimate of $\hat{V}_{min}$ is $\hat{V}$ evaluated at θ_{max} and λ_{min}, and an overestimate of $\hat{\Psi}_{max}$, denoted by $\hat{\Psi}_{MAX}$, is $\hat{\Psi}$ evaluated at θ_{min} and λ_{min} and maximized (numerically) over the range $\hat{\omega}_{LC}$ to $\hat{\omega}_{UC}$. Thus all λ values small enough that

$$(v/c)^2(\omega_{pe0}/\Omega_{e0})^2 H(\lambda)\cos^2\theta_{max} > \hat{\Psi}_{MAX} \qquad (21)$$

will satisfy $V_{min} > \Psi_{max}$. Similarly, all λ values large enough that

$$(v/c)^2(\omega_{pe0}/\Omega_{e0})^2 H(\lambda)\cos^2\theta_{min} < \hat{\Psi}_{MIN}, \qquad (22)$$

where $\hat{\Psi}_{MIN}$ is $\hat{\Psi}$ evaluated at θ_{max} and λ_{max} and minimized over $\hat{\omega}_{LC}$ to $\hat{\omega}_{UC}$, will satisfy $V_{max} < \Psi_{min}$. These λ ranges will have no resonances within the imposed θ and ω ranges and cannot contribute to the bounce-averaged diffusion coefficients. A further restriction on λ is found in section 7.

[32] The analysis may be extended to $n \neq 0$ to restrict λ ranges and, following section 5.1.2, to identify maximum values of $|n|$ beyond which there are no resonances at any accessible λ.

6. Finding Eligible Resonances

[33] After eliminating as much of the θ and λ integrals as possible, the remaining θ ranges must be integrated over according to equation (5); to do this, the resonances that do in fact lie between the cutoff frequencies must be found. A straightforward approach is to derive a polynomial $P(\omega)$ from the resonance condition [*Glauert and Horne*, 2005], which turns out to be 10th order in ω. Instead, the geometric analysis of V and Ψ presented above may be used to try to bracket the frequencies, which are then found with any one-dimensional root finding algorithm [e.g., *Press et al.*, 1992]. The simplest situation is where $V'(\omega)$ and $\Psi'(\omega)$ have

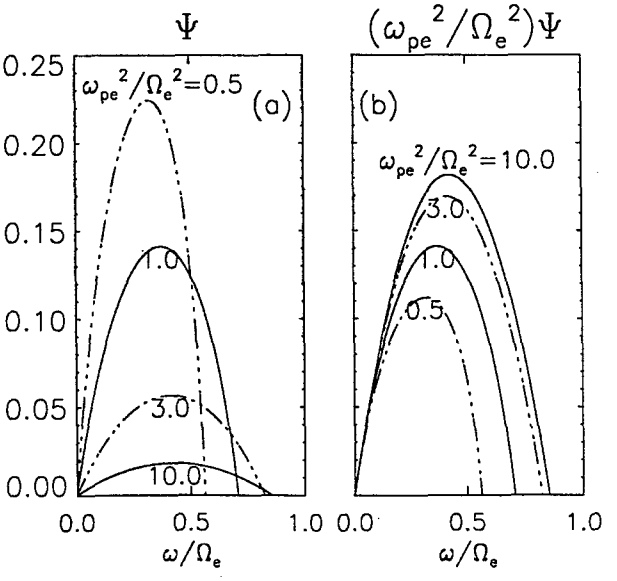

Figure 6. The functions (a) Ψ and (b) $(\omega_{pe}^2/\Omega_e^2)\Psi$ versus ω/Ω_e for different values of ω_{pe}^2/Ω_e^2, with $\theta = 30°$.

opposite signs everywhere between the cutoffs, since then V and Ψ can intersect at most once (and will do so only if $V(\omega_{LC}) - \Psi(\omega_{LC})$ and $V(\omega_{UC}) - \Psi(\omega_{UC})$ have opposite signs). Otherwise, if V' and Ψ' have the same signs but V'' and Ψ'' have opposite signs, then V' and Ψ' can have at most one intersection, which separates possible intersections of V with Ψ. These cases are identified below.

6.1. Case $n = 0$

[34] This is the simplest case because V does not depend on ω. For $\theta > \theta_{sep}$, $\Psi(\omega)$ is always decreasing so can intersect V only once. For $\theta < \theta_{sep}$, there will be at most two intersections of $\Psi(\omega)$ with V, separated by ω_{peak}. In fact, ω_{peak} will only lie between ω_{LC} and ω_{UC} for $\Theta_{UC} < \theta < \Theta_{LC}$. For other θ values, $\Psi(\omega)$ is always either increasing or decreasing between the cutoffs and intersects $V(\omega)$ there exactly once (the θ values for which these intersections are outside the cutoffs have already been eliminated).

6.2. Case $\omega_n > 0$

[35] There are several subcases. First, for $\theta > \theta_{sep}$, Ψ is always decreasing, so it can intersect the rising branch of V (where $\omega < \omega_n$) at most once. An intersection with the decreasing branch of V would require $\omega_n < \Omega_{gm}$ so that $\gamma > 1/\sqrt{M}$ or $E > 20$ MeV (for electrons), which is not considered here.

[36] Otherwise, Ψ is either rising or has negative curvature. The falling branch of V has positive curvature, so it could intersect Ψ at most twice, with the two intersections separated by the single root of $V' - \Psi'$. Of course these roots need only be sought between $\max(\omega_n, \omega_{LC})$ and ω_{UC}.

[37] Since the rising branch of V also has positive curvature and starts out below Ψ at $\omega = 0$, it can intersect Ψ at most once in the range $\omega > \omega_{infl}$ where Ψ has negative curvature. However, if the rising branch of V intersects Ψ at $\omega < \omega_{infl}$, both curves are rising and have positive curvature so multiple intersections must be considered. This is analogous to the situation of section 3.2.1 of Paper 1 and is resolved the same way: V' is necessarily greater than Ψ' at the first such intersection ω_*, and $\partial V/\partial\omega$ increases faster than linearly, so even the function $(\partial V/\partial\omega)/\omega$ is increasing with ω. However, even when $\partial\Psi/\partial\omega$ is increasing, $(\partial\Psi/\partial\omega)/\omega$ is decreasing (for all ω, verified numerically). Thus V' increases faster than Ψ' for $\omega > \omega_*$, and this branch of V cannot intersect Ψ again. In summary, there are at most three intersections: one for the rising branch of V and two for the falling branch.

6.3. Case $\omega_n < 0$

[38] As in section 3.3 of Paper 1, this is the most problematic situation. Cases where either $V'(\omega)$ and $\Psi'(\omega)$, or else V'' and Ψ'', have opposite signs everywhere between the cutoffs can be handled as above. However, V and Ψ both have positive slope and positive curvature for $\omega < \min(\omega_{infl}, |\omega_n|/2)$ (so that $\omega_{LC} < \omega_{LH}$), and they both have positive slope and negative curvature for $\max(\omega_{infl}, |\omega_n|/2) < \omega < \omega_{peak}$ (so that $|n| < \gamma \cos\theta_{min}$). If the preceding tests do not rule out these possibilities, then no convenient argument is known to bracket the roots of $V - \Psi$, as was done above for $\omega_n > 0$ or in section 3.3 of Paper 1.

[39] In principle, Sturm's theorem gives the exact number of real roots of the polynomial $P(\omega)$ in any range (ω_1, ω_2) in terms of the number of alternations in sign of sequences of polynomials derived from $P(\omega)$ and evaluated at ω_1 and ω_2 [e.g., *Barbeau*, 2003]. However, since the 11 coefficients of $P(\omega)$ depend on the parameters ω_{pe}/Ω_e, θ, γ, α, and n (as do the coefficients of the derived polynomials), a general characterization of these signs has not been attempted. Descartes' rule of signs and the theorem of Fourier and Budan are similar but less definitive and almost as difficult to apply.

[40] To proceed, one option is to revert to the polynomial $P(\omega)$ for $\omega(\theta)$, accepting the inefficiency that the solutions will not necessarily lie between ω_{LC} and ω_{UC}. Also, the (real) solutions must be checked to verify that they satisfy the original equation $V = \Psi$. An alternative is to integrate $\mathcal{D}^{\mu\kappa}$ over ω instead, finding $\theta(\omega)$ easily via a quadratic in $\cos^2\theta$ as mentioned in section 5; this accepts the analogous inefficiency that much of the ω range will likely yield θ values outside the range θ_{min} to θ_{max} and sacrifices the elimination of any θ ranges that are possible for this particular value of ω_n.

7. Dependence of D_{pp} on Density Ratio

[41] The ratio of momentum diffusion to pitch angle diffusion is controlled by equation (4), which may be written as

$$\Delta \equiv \frac{\mathcal{D}^{\mu\kappa}_{pp}}{\mathcal{D}^{\mu\kappa}_{\alpha\alpha}} = \frac{\cos^2\alpha}{\sin^2\alpha}\frac{\omega^2}{(\omega-\Omega_n)^2}, \quad \Omega_n = \frac{\omega_n}{\sin^2\alpha}. \tag{23}$$

This is the same dependence on ω as in equation (10) for $V(\omega)$, with the similar result that Δ increases with increasing ω for $\Omega_n < 0$ or $\omega < \Omega_n$ and decreases with increasing ω for $0 < \Omega_n < \omega$.

[42] As ω_{pe}/Ω_e decreases, Figure 6a shows that Ψ increases for $\omega < \omega_{peak}$ while the V curve is unchanged, so (from Figures 1 or 5a) the resonant frequency will increase where $\partial V/\partial\omega > 0$ and vice versa. Thus for $\omega_n < 0$ or $\omega < \omega_n$, decreasing ω_{pe}/Ω_e means typical ($<\omega_{peak}$) resonant ω values increase and Δ increases; for $\omega > \Omega_n$, decreasing ω_{pe}/Ω_e means typical resonant ω values decrease and Δ increases.

[43] The only remaining case is $0 < \omega_n < \omega < \Omega_n$, but such resonances do not seem to be possible. (Figure 5a shows two resonances with $0 < \omega_n < \omega$, but the parameters are such that $\omega > \Omega_n$.) This statement is proved in Appendix B with the restriction $\omega_{pe}/\Omega_e > 1/2$. Extensive numerical tests (looking for valid solutions to the quadratic for $\sin^2\theta$ for over 10^{10} combinations of ω, ω_{pe}/Ω_e, γ, α, and n) indicate that it holds for all values $\omega_{pe}/\Omega_e > 10^{-3}$ (the lowest value tested).

[44] This finding can also be used to increase the effectiveness of the methods of section 5.1, since for $\omega_n > 0$, only the parts of the interval $(\omega_{LC}, \omega_{UC})$ outside (ω_n, Ω_n) need be considered. This finding could further be used to to eliminate some λ ranges, as in section 5.3; for $\omega_n > 0$, values of λ for which the interval $(\omega_{LC}, \omega_{UC})$ lies within (ω_n, Ω_n) can be omitted.

8. Results

[45] Bounce-averaged results based on models of CRRES wave data covering three different local time

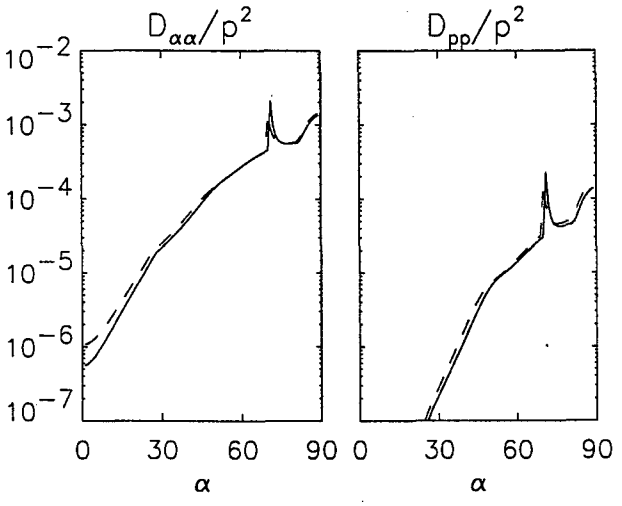

Figure 7. Local (equatorial) diffusion coefficients $D_{\alpha\alpha}$ and D_{pp} for a 1 MeV electron with $\omega_{pe}/\Omega_e = 1.5$, $\omega_m = 0.35$, $\delta\omega = 0.15$, $\omega_{LC} = 0.05$, and $\omega_{UC} = 0.65$ (after *Horne et al.* [2003]). The solid curves are based on the full whistler dispersion relation while the dashed curves use the high density approximation.

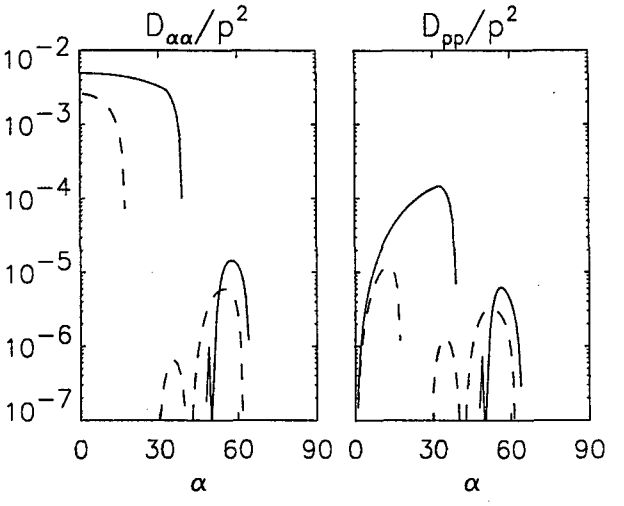

Figure 9. Diffusion coefficients for a 1 MeV electron as in Figure 7 with $\omega_{pe}/\Omega_e = 0.5$, $\omega_m = 0.1$, $\delta\omega = 0.05$, $\omega_{LC} = 0.05$, and $\omega_{UC} = 0.15$.

sectors [*Meredith et al.*, 2001] were presented by *Horne et al.* [2005]. The diffusion coefficients were calculated by two independent codes, one described by *Glauert and Horne* [2005] and one based on the analysis presented above. In this section, the reliability of the high-density approximation is explored. Also, the gain in computational efficiency of the present methods is demonstrated.

8.1. Comparison to the High-Density Approximation

[46] Local diffusion coefficients were calculated for 1 MeV electrons with the same parameters as in the work of *Horne et al.* [2003], namely $B^2(\omega)$, a gaussian of ω/Ω_e centered at $\omega_m = 0.35$ with halfwidth $\delta\omega = 0.15$ and cutoffs $\omega_{LC} = 0.05$ and $\omega_{UC} = 0.65$, and $g_\omega(\theta)$, a gaussian of tan θ centered at $x_m = 0$ with halfwidth $x_w = \tan 30°$ and cutoffs $x_{\min} = 0$ and $x_{\max} = 1$. For $\omega_{pe}/\Omega_e = 10$, 7.5, 5, and 2.5, the values obtained for $D_{\alpha\alpha}$ and D_{pp} effectively duplicate Figures 2 and 3 of *Horne et al.* [2003]. Agreement was also obtained for $\omega_{pe}/\Omega_e = 1.5$, although this required lowering $x_{\max}$ to slightly less than (i.e., 0.999 times) the resonance cone value. Rather surprisingly, the values obtained using the form of the diffusion coefficients based on the high density approximation, computed as in Paper 1, are essentially identical for $\omega_{pe}/\Omega_e > 1.5$ and almost the same for $\omega_{pe}/\Omega_e = 1.5$ (which in the high density approximation does not involve the resonance cone), as shown in Figure 7. Figure 8 shows another comparison, with the normalized frequency parameters changed to $\omega_{pe}/\Omega_e = 1$, $\omega_m = 0.4$, $\delta\omega = 0.1$, $\omega_{LC} = 0.3$, and $\omega_{UC} = 0.5$ (this avoids the resonance cone); the high-density approximation holds up quite well except at low values of α. Figure 9 shows a comparison with $\omega_{pe}/\Omega_e = 0.5$, $\omega_m = 0.1$, $\delta\omega = 0.05$, $\omega_{LC} = 0.05$, and $\omega_{UC} = 0.15$; here, the high-density approximation is not reliable.

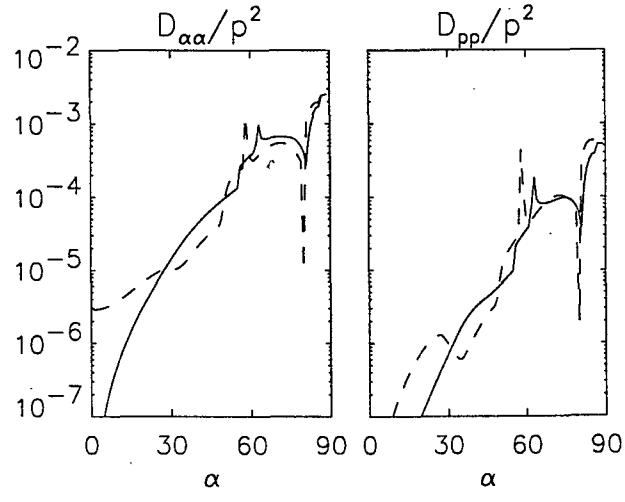

Figure 8. Diffusion coefficients for a 1 MeV electron as in Figure 7 with $\omega_{pe}/\Omega_e = 1$, $\omega_m = 0.4$, $\delta\omega = 0.1$, $\omega_{LC} = 0.3$, and $\omega_{UC} = 0.5$.

8.2. Computational Efficiency

[47] The amount of computer time needed to perform these calculations varies greatly with the various physical parameters, as well as numerical details. The test case used here is the calculation of bounce-averaged diffusion rates for 1 MeV electrons at L = 4.5 in the night sector, with $-5 \le n \le 5$, as presented by *Horne et al.* [2005]. (Models for the other sectors considered in that paper approach the resonance cone.) The CPU times reported are for totals for $\alpha_0 = 89°, 88°, \ldots, 5°$ (just outside the loss cone). To perform numerical integrations, the code described here relied on Romberg's method, adapted from the implementation of *Press et al.* [1992]. The calculations were performed as $\int d\lambda \sum_n \int dx D^{nx}$, where $x = \tan\theta$. As a baseline, the resonant frequencies $\omega(\theta)$ were found by solving the polynomial $P(\omega)$ discussed in section 6.3, regardless of n, without using any of the analysis above. As expected, this way was the slowest. Then the techniques of sections

Table 1. CPU Times, s

	$P(\omega)$		$V = \Psi$	
E, MeV	All θ	Restricted	All θ	Restricted
		$\lvert n \rvert \leq 5$		
0.01	419.0	86.4	147.4	54.5
0.03	366.2	91.0	119.6	51.3
0.1	364.7	164.7	127.3	86.2
0.3	389.8	263.4	166.5	140.5
1.0	508.3	421.0	235.1	204.0
		$\lvert n \rvert \leq 20$		
0.01	1248.5	86.4	385.2	54.5
0.03	1165.5	90.4	337.0	51.3
0.1	1144.3	165.5	340.6	87.3
0.3	1231.9	331.7	386.7	172.4
1.0	1551.3	834.5	540.1	396.3

5.1 and 5.2 were used to cut down the ranges of θ; over the ranges not skipped, the resonances were again found using $P(\omega)$. This produced the same values (within a few percent) in considerably less time. Next, solving $P(\omega)$ for the resonances was replaced by solving $V = \Psi$ but, as an experiment, the integral over wavenormal angle was done over the whole range 0 to x_{max}. This also sped up the calculations (sometimes by more, sometimes by less). Finally, the techniques of restricting the θ ranges and solving $V = \Psi$ were combined, yielding the fastest method. The timing results are shown in Table 1. Generally speaking, lower-energy particles have fewer resonances, so there is more opportunity to avoid nonresonant values of θ, n, and λ. For the same reason, the techniques will be more effective the smaller the range of allowed resonances, ω_{LC} to ω_{UC}.

[48] Because of the decreased computer time, it is feasible to consider larger values of n. For large E and small α_0, it turns out that resonances are present with n as large as ± 23, although the addition to the total diffusion coefficients is only a few percent. Moreover, the method discussed in section 5.1.2 to estimate the maximum $|n|$ needed at each α_0 and λ was very effective, typically overestimating $|n_{max}|$ by only 2 or 3. Thus the code takes only a little longer to include, in effect, $-\infty \leq n \leq \infty$. Because the simplest method behaves especially badly when n is too large for resonance, Table 1 shows timing comparisons with $-20 \leq n \leq 20$.

[49] As mentioned, these timings are highly dependent on the parameters of the problem and on the numerical procedure. However, it is clear that the analysis and techniques presented here can greatly increase the efficiency and practicality of the calculations and (for a given amount of computer time) improve their accuracy.

9. Summary

[50] For whistler mode waves, a detailed characterization was given of $\Psi = 1/\mu^2$ versus ω, treating θ as a parameter. Ψ was shown to have no internal minima and a single local maximum whose location ω_{peak} decreases monotonically with θ, as does $\Psi(\omega_{peak})$. For a given range ω_{LC} to ω_{UC}, this determines the value of Ψ_{min}, as well as the value of Ψ_{max} when $\Psi(\omega_{peak})$ lies outside the frequency range. Several estimates were given for Ψ_{max} when ω_{peak} lies inside the frequency range, including one based on the factorization of Ψ into increasing and decreasing functions and one based on the high density approximation.

[51] The minimum and maximum values of the function $V(\omega)$ were also found, which leads to conditions on θ (equation (19)) for the existence of solutions to the resonance condition, $V = \Psi$. This and related constraints on θ ranges can be used to drastically reduce the amount of integration over θ required to evaluate quasi-linear diffusion coefficients. A maximum value of $|n|$ can be determined for which there are any resonances at all. This approach can also be extended to identify ranges of latitude λ which contain no resonances; this was carried out in detail for the case $n = 0$.

[52] For variable and parameter ranges that do contribute to the diffusion rates, with $\omega_n \geq 0$ it was possible to both enumerate the resonant frequencies and to isolate them, i.e., to find expressions that bracket and separate them so that they can easily be found numerically. For cases with $\omega_n < 0$ that cannot be eliminated, a 10th order polynomial must be solved for $\omega(\theta)$ or else the integration performed over ω, which only requires solving a quadratic for $\sin^2\theta$ as a function of ω. These techniques were used to evaluate diffusion coefficients for relativistic electrons at L = 4.5 using realistic models of the wave parameters, as reported by *Horne et al.* [2005].

[53] It should also be relatively straightforward to modify this analysis for other types of plasma waves. In particular, Z modes can resonate with energetic electrons [*Horne and Thorne*, 1998] and have a refractive index that is quite similar to that of the whistler mode [e.g., *Carpenter et al.*, 2003].

[54] A brief analysis was given of the typically increasing relative strength of momentum diffusion, $D_{pp}/D_{\alpha_0\alpha_0}$, with decreasing density ratio ω_{pe}/Ω_e. In passing it was observed that for $\omega_n > 0$ ($n < 0$ for electrons), a particle with pitch angle α has no resonances between ω_n and $\omega_n/\sin^2\alpha$. It is tempting to speculate that this is somehow related to the gap in chorus wave spectra frequently observed at $\Omega_e/2$ [e.g., *Anderson and Maeda*, 1977].

[55] Calculations using the full whistler dispersion relation were compared to results with the widely used high-density approximation. In the cases chosen, this approximation was found to be quite reliable for density ratio $\omega_{pe}/\Omega_e > 1$ and qualitatively good at $\omega_{pe}/\Omega_e = 1$ except at low pitch angle but failed badly at $\omega_{pe}/\Omega_e = 0.5$. Finally, the computational effectiveness of the analysis was demonstrated, decreasing the computer time significantly for calculations with $-5 \leq n \leq 5$ and even more so for $-20 \leq n \leq 20$. Since the analysis is able to accurately estimate the maximum $|n|$ for which resonances occur, it is possible to take, in effect, $-\infty \leq n \leq \infty$.

Appendix A: Proofs of Some Properties of the Function Ψ

[56] For whistler mode waves, with $P < 0$ and $R > 0$, Ψ can be written as

$$Y \sin^2\theta + S/RL - \sigma\sqrt{Y^2 \sin^4\theta + (D/RL)^2 \cos^2\theta}, \qquad \text{(A1)}$$

where $Y = (RL - PS)/2PRL$ and σ is the sign of DL. Taking the (partial) derivative of Ψ with respect to any of the parameters of (R, L, P) gives

$$\Psi' = Y' \sin^2\theta + (S/RL)' - \sigma \frac{YY' \sin^4\theta + (D/RL)(D/RL)' \cos^2\theta}{\sqrt{Y^2 \sin^4\theta + (D/RL)^2 \cos^2\theta}}. \quad \text{(A2)}$$

This may be rewritten as

$$\Psi' = -\frac{P'}{2P^2} \sin^2\theta(1 - \cos\phi) - \frac{R'}{R^2} \cos\theta \sin\phi + \left(\frac{S}{RL}\right)' \left[1 - \frac{\sin^2\theta}{2}(1 - \cos\phi) - \cos\theta \sin\phi\right], \quad \text{(A3)}$$

where

$$\{\cos\phi,\ \sin\phi\} \equiv \frac{\{\sigma Y \sin^2\theta, |D/RL| \cos\theta\}}{\sqrt{Y^2 \sin^4\theta + (D/RL)^2 \cos^2\theta}}$$

and $\cos\theta \sin\phi \geq 0$. With θ and ϕ considered as independent variables, $0 \leq \theta, \phi \leq \pi$, it can be shown that the bracketed term in (A3) is never less than 0. The form (A3) leads to proofs of three assertions concerning Ψ made in the text, as shown below.

A1. Proof That $\Psi > \Psi^{(M=0)}$

[57] Taking $\Psi' = \partial\Psi/\partial M$, it is readily checked that P' and R' are negative and $(S/RL)'$ is positive. Therefore $\partial\Psi/\partial M$ is never negative, which proves $\Psi > \Psi^{(M=0)}$ as claimed in section 4.2.

A2. Proof That $\Psi < \Psi^{HD}$

[58] Next, replace the leading "1" in the definitions of R, L, and P with an additional parameter β, so that the exact Ψ is given by $\beta = 1$ and the high density approximation Ψ^{HD} is given by $\beta = 0$. With $\Psi' = \partial\Psi/\partial\beta$, (A3) is unchanged but now P' and R' are positive. Therefore Ψ' will be negative if $(S/RL)'$ is negative. Evaluating $(S/RL)'$ gives a quadratic function $f(\beta)$ divided by a positive (squared) function. (A computer algebra program, such as Mathematica [*Wolfram*, 2003], is useful here.) Both the leading coefficient and the discriminant of $f(\beta)$ turn out to be negative so f is downward-facing, with no real roots. Thus f is always negative, $(S/RL)'$ is negative, and $\partial\Psi/\partial\beta < 0$, which proves $\Psi < \Psi^{HD}$ as claimed in section 4.1.

A3. Proof That $(\omega_{pe}^2/\Omega_e^2)\Psi$ Increases as ω_{pe}^2/Ω_e^2 Increases

[59] Finally, consider $\tilde{\Psi} = (\omega_{pe}^2/\Omega_e^2)\Psi$. Let ρ denote Ω_e^2/ω_{pe}^2, and define $(\tilde{R}, \tilde{L}, \tilde{P})$ as $(\rho R, \rho L, \rho P)$. Then the form of $\tilde{\Psi}(\tilde{R}, \tilde{L}, \tilde{P})$ is exactly the same as that of $\Psi(R, L, P)$ in (A1). Furthermore, since

$$\tilde{P} = \rho - (1 + M)/\omega^2,$$

and similarly for R and L, here ρ plays the same algebraic role in $\tilde{\Psi}$ as β did in Ψ. The calculation of $\partial\tilde{\Psi}/\partial\rho < 0$ proceeds exactly like that of $\partial\Psi/\partial\beta < 0$, with the result that $\tilde{\Psi}$ increases as ρ decreases and ω_{pe}^2/Ω_e^2 increases, as claimed in section 5.3.

Appendix B: Absence of Resonances Between ω_n and Ω_n

[60] With $\omega_{pe}/\Omega_e > 1/2$, it is readily proved that there are no resonances between $\omega_n = |n|\Omega_e/\gamma$ and $\Omega_n = \omega_n/\sin^2\alpha$. Since $\Psi < \Psi^{HD}$,

$$\Psi_{\max} < \frac{\Omega_e^2}{\omega_{pe}^2} \frac{\cos^2\theta}{4} < \cos^2\theta. \quad \text{(B1)}$$

If $\Omega_n < \Omega_e$ then $1/\gamma^2 < \sin^4\alpha/n^2$, and evaluating V at $\omega = \Omega_n$ gives

$$V_{\min} > \frac{1 - \sin^4\alpha/n^2}{1 - \sin^2\alpha} \cos^2\theta > \cos^2\theta. \quad \text{(B2)}$$

If, on the other hand, $\Omega_n > \Omega_e > \omega_n$, then $\cos^2\alpha > 1 - |n|/\gamma$ and evaluating V at $\omega = \Omega_e$ (recall $\Psi < 0$ for larger ω) gives

$$V_{\min} > \frac{\gamma - 1/\gamma}{\gamma - |n|} \cos^2\theta > \cos^2\theta. \quad \text{(B3)}$$

In either case, $V_{\min} > \Psi_{\max}$, so there can be no solutions to $V = \Psi$.

[61] **Acknowledgments.** This work was supported by the Space Vehicles Directorate of the Air Force Research Laboratory and by the National Science Foundation under grant 0317320. The author thanks S. L. Young for a careful reading of the manuscript.

[62] Shadia Rifai Habbal thanks Clare E. J. Watt and Yoshiharu Omura for their assistance in evaluating this paper.

References

Albert, J. M. (1999), Analysis of quasi-linear diffusion coefficients, *J. Geophys. Res.*, *104*(A2), 2429.

Albert, J. M. (2000), Gyroresonant interactions of radiation belt particles with a monochromatic electromagnetic wave, *J. Geophys. Res.*, *105*(A9), 21,191.

Albert, J. M. (2001), Comparison of pitch angle diffusion by turbulent and monochromatic whistler waves, *J. Geophys. Res.*, *106*(A5), 8477.

Albert, J. M. (2002), Nonlinear interaction of outer zone electrons with VLF waves, *Geophys. Res. Lett.*, *29*(8), 1275, doi:10.1029/2001GL013941.

Albert, J. M. (2003), Evaluation of quasi-linear diffusion coefficients for EMIC waves in a multi-species plasma, *J. Geophys. Res.*, *108*(A6), 1249, doi:10.1029/2002JA009792.

Albert, J. M. (2004), Analytical bounds on the whistler mode refractive index, *Phys. Plasmas*, *11* 4875, doi:10.1063/1.1792634.

Anderson, R. R., and K. Maeda (1977), VLF emissions associated with enhanced magnetospheric electrons, *J. Geophys. Res.*, *82*, 135.

Barbeau, E. J. (2003), *Polynomials*, Springer, New York.

Carpenter, D. L., T. F. Bell, U. S. Inan, R. F. Benson, V. S. Sonwalkar, B. W. Reinisch, and D. L. Gallagher (2003), Z-mode sounding within propagation "cavities" and other magnetospheric regions by the RPI instrument on the IMAGE satellite, *J. Geophys. Res.*, *108*(A12), 1421, doi:10.1029/2003JA010025.

Glauert, S. A., and R. B. Horne (2005), Calculation of pitch angle and energy diffusion coefficients with the PADIE code, *J. Geophys. Res.*, doi:10.1029/2004JA010851, in press.

Horne, R. B., and R. M. Thorne (1998), Potential waves for relativistic electron scattering and stochastic acceleration during magnetic storms, *Geophys. Res. Lett.*, *25*(15), 3011.

Horne, R. B., S. A. Glauert, and R. M. Thorne (2003), Resonant diffusion of radiation belt electrons by whistler-mode chorus, *Geophys. Res. Lett.*, *30*(9), 1493, doi:10.1029/2003GL016963.

Horne, R. B., R. M. Thorne, S. A. Glauert, J. M. Albert, N. P. Meredith, and R. R. Anderson (2005), Timescale for radiation belt electron acceleration by whistler mode chorus waves, *J. Geophys. Res.*, doi:10.1029/2004JA010811, in press.

Lyons, L. R. (1974a), General relations for resonant particle diffusion in pitch angle and energy, *J. Plasma Phys.*, *12*, 45.

Lyons, L. R. (1974b), Pitch angle and energy diffusion coefficients from resonant interactions with ion-cyclotron and whistler waves, *J. Plasma Phys.*, *12*, 417.

Lyons, L. R., R. M. Thorne, and C. F. Kennel (1972), Pitch-angle diffusion of radiation belt electrons within the plasmasphere, *J. Geophys. Res.*, *77*, 3455.

Meredith, N. P., R. B. Horne, and R. R. Anderson (2001), Substorm dependence of chorus amplitudes: Implications for the acceleration of electrons to relativistic energies, *J. Geophys. Res.*, *106*(A7), 13,165.

Press, W. H., S. A. Teukolsky, W. T. Vetterling, and B. P. Flannery (1992), *Numerical Recipes*, Cambridge Univ. Press, New York.

Santolik, O., D. A. Gurnett, J. S. Pickett, M. Parrot, and N. Cornilleau-Wehrlin (2003), Spatio-temporal structure of storm-time chorus, *J. Geophys. Res.*, *108*(A7), 1278, doi:10.1029/2002JA009791.

Sazhin, S. S., and M. Hayakawa (1992), Magnetospheric chorus emissions: A review, *Planet. Space Sci.*, *40*(5), 681.

Smith, A. J., and D. Nunn (1998), Numerical simulation of VLF risers, fallers, and hooks observed in Antarctica, *J. Geophys. Res.*, *103*(A4), 6771.

Stix, T. H. (1962), *The Theory of Plasma Waves*, McGraw-Hill, New York.

Summers, D., and C. Ma (2000), A model for generating relativistic electrons in the Earth's inner magnetosphere based on gyroresonant wave-particle interactions, *J. Geophys. Res.*, *105*(A2), 2625.

Summers, D., R. M. Thorne, and F. Xiao (1998), Relativistic theory of wave-particle resonant diffusion with application to electron acceleration in the magnetosphere, *J. Geophys. Res.*, *103*(A9), 20,487.

Trakhtengerts, V. Y., M. J. Rycroft, D. Nunn, and A. G. Demekhov (2003), Cyclotron acceleration of radiation belt electrons by whistlers, *J. Geophys. Res.*, *108*(A3), 1138, doi:10.1029/2002JA009559.

Wolfram, S. (2003), *Mathematica*, Wolfram Media, Inc., Champaign, Ill.

J. M. Albert, Air Force Research Laboratory/VSBX, 29 Randolph Road, Hanscom AFB, MA 01731-3010, USA. (jay.albert@hanscom.af.mil)